

# Timescales for detection of trends in the ocean carbon sink

Galen A. McKinley<sup>1,2,3</sup>, Darren J. Pilcher<sup>1,4</sup>, Amanda R. Fay<sup>3</sup>, Keith Lindsay<sup>5</sup>, Matthew C. Long<sup>5</sup> & Nicole S. Lovenduski<sup>6</sup>

**The ocean has absorbed 41 per cent of all anthropogenic carbon emitted as a result of fossil fuel burning and cement manufacture<sup>1,2</sup>. The magnitude and the large-scale distribution of the ocean carbon sink is well quantified for recent decades<sup>3,4</sup>. In contrast, temporal changes in the oceanic carbon sink remain poorly understood<sup>5–7</sup>. It has proved difficult to distinguish between air-to-sea carbon flux trends that are due to anthropogenic climate change and those due to internal climate variability<sup>5,6,8–13</sup>. Here we use a modelling approach that allows for this separation<sup>14</sup>, revealing how the ocean carbon sink may be expected to change throughout this century in different oceanic regions. Our findings suggest that, owing to large internal climate variability, it is unlikely that changes in the rate of anthropogenic carbon uptake can be directly observed in most oceanic regions at present, but that this may become possible between 2020 and 2050 in some regions.**

Recent observationally based syntheses have quantified mean ocean carbon uptake and its spatial distribution<sup>1,3,4,15</sup> (Extended Data Fig. 1). In addition, interior ocean observations analysed under the assumption of constant ocean circulation suggest a steady increase in the integrated sink over the last century<sup>1,15</sup>. Yet surface observations clearly indicate that carbon uptake is strongly affected by variability in surface climate and ocean circulation<sup>5,8–13</sup>. This variability impedes our ability to develop a detailed, regional picture of how the ocean carbon sink is changing in response to increasing atmospheric partial pressure of carbon dioxide ( $p_{\text{CO}_2}$ ) and the associated climate change. Although climate models suggest that the ocean should be a net sink for anthropogenic carbon for at least the next several centuries, they also suggest that climate warming and circulation changes will act to reduce the sink's magnitude<sup>7,16</sup>. Monitoring current and future effects from the combined impact of increasing atmospheric  $p_{\text{CO}_2}$  and climate change—that is, the forced trend—on ocean carbon uptake presents a major observational challenge due to the strong influence of the variability inherent to the climate system<sup>14,17,18</sup>.

Previous modelling studies have attempted to separate internal variability from forced trends in ocean carbon uptake using several approaches. Variability in air-to-sea carbon fluxes has been linked to modes of climate variability in realistic hindcast models<sup>19–21</sup>. However, anthropogenic change can project onto these modes, leading to an incomplete separation. The ocean's response to increasing atmospheric CO<sub>2</sub> in the absence of variability and change has been studied<sup>13</sup>, but this approach ignores both mean impacts on ocean circulation from variable climate and indirect impacts on the carbon sink due to circulation change. Collections of Earth System Models have been used to assess relationships between natural variability and carbon cycle trends<sup>22,23</sup>, but diverse model structures—for example, the spatial resolution of the atmosphere and ocean components, parameterization of the lower food web, or numerical schemes—can influence resulting trends<sup>24</sup>. Structural uncertainty precludes clear identification of the influence of internal variability<sup>24</sup>.

We make use here of a large ensemble of a single Earth system model, the Community Earth System Model—Large Ensemble (CESM-LE, ref. 25) to assess variability and change in the ocean carbon cycle in recent decades and through 2100. CESM is a comprehensive coupled climate model consisting of atmosphere, ocean, land surface, and sea ice components. The CESM-LE experiment includes 32 members with ocean biogeochemistry output. The experiment included a control integration of >2,000 years. A transient integration (ensemble member 1) started at year 402 of the control and was integrated for 251 years under historical forcing (1850–2005) and then the Intergovernmental Panel on Climate Change Representative Concentration Pathway (IPCC RCP) 8.5 scenario for 2006–2100. Additional ensemble members were initialized from ensemble member 1 at 1 January 1920, with round-off level perturbations applied to the air temperature field. See Methods for more details.

Here, the use of a single model eliminates structural differences inherent to multi-model ensembles<sup>24</sup>, allowing the spread across the ensemble to be wholly attributed to the internal variability of the modelled climate system<sup>14,17,18,26</sup>. For each ensemble member, temporal trends in any variable can be separated into two parts: (1) the forced trend that is common across all ensembles, and (2) the unforced, or internal trend, that occurs only in that ensemble member. The spread of trends across the ensemble indicates how much internal variability causes individual ensemble members to deviate from the forced trend<sup>14,17,18,26</sup>. The forced trend, as its name suggests, is due to the model forcing, here including anthropogenic greenhouse gases and aerosols, as well as natural forcings (for example, solar variability and volcanoes) during the historical period<sup>14,25</sup>. In the case of the ocean carbon sink, there are two components to the forced trend. The first is the direct influence of increasing atmospheric  $p_{\text{CO}_2}$  driving continued ocean carbon uptake. The second is the indirect effect of changing climate that influences the physical state of the ocean and modulates air-to-sea carbon fluxes.

Comparisons to observations illustrate that CESM captures the dominant modes and magnitudes of ocean carbon cycle variability and trends at regional to global scales (ref. 21, Methods, Extended Data Tables 1 and 2). To further validate the simulated mean CO<sub>2</sub> flux, we compare to fluxes estimated from observations<sup>5</sup>, and to a multi-model ensemble of 12 Coupled Model Intercomparison Project 5 (CMIP5) Earth system models (Fig. 1, Extended Data Fig. 1, Extended Data Table 3). For the 30-year mean CO<sub>2</sub> flux, CESM-LE is consistent with the observed estimates in most regions and for the global average, with small differences across the individual ensemble members (Fig. 1). In contrast, there is a substantial spread in CO<sub>2</sub> flux estimates from CMIP5<sup>23</sup>. It is to be expected that structural differences between models would dominate differences in the multi-decadal mean CO<sub>2</sub> flux, since the long averaging period integrates over the timescales of the dominant modes of variability. This is exactly what we find; a much greater spread in mean CO<sub>2</sub> flux for CMIP5 than for CESM-LE for all biomes

<sup>1</sup>Department of Atmospheric and Oceanic Sciences, University of Wisconsin—Madison, Madison, Wisconsin, USA. <sup>2</sup>Center for Climatic Research, University of Wisconsin—Madison, Madison, Wisconsin, USA. <sup>3</sup>Space Science and Engineering Center, University of Wisconsin—Madison, Madison, Wisconsin, USA. <sup>4</sup>NOAA Pacific Marine Environmental Laboratory, Seattle, Washington, USA.

<sup>5</sup>National Center for Atmospheric Research, Boulder, Colorado, USA. <sup>6</sup>Department of Atmospheric and Oceanic Sciences and Institute of Arctic and Alpine Research, University of Colorado Boulder, Boulder, Colorado, USA.

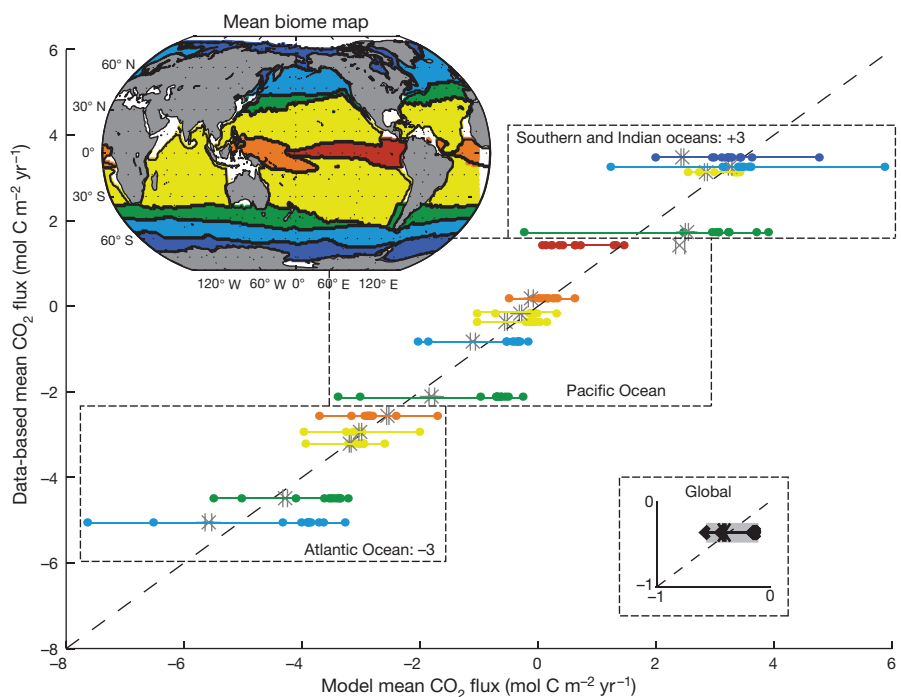


**Figure 1 | Modelled and observed mean 1982–2011 CO<sub>2</sub> flux in 15 ocean biomes.** The CESM-LE mean is shown as a grey cross, with max/min in grey ( $N=32$ ), aligned with horizontal lines for each biome. Coloured dots represent CMIP5 models ( $N=12$ ), corresponding to the biome colours on the inset mean biome map (ICE, dark blue; SPSS, light blue; STSS, green; STPS, yellow; EQ, orange and red; full names are given in

Extended Data Table 4). There is insufficient data to plot the Northern Hemisphere ICE biomes<sup>28</sup>. The Atlantic Ocean is offset by  $-3 \text{ mol C m}^{-2} \text{ yr}^{-1}$ , and the Southern and Indian oceans by  $+3 \text{ mol C m}^{-2} \text{ yr}^{-1}$ . The global mean is shown in the bottom right inset (scale is twice that of the main panel); the uncertainty on the observed value (grey band) is  $0.12 \text{ mol C m}^{-2} \text{ yr}^{-1}$  (ref. 28; P. Landschützer, personal communication).

(Fig. 1). These structural differences across CMIP5 also affect CO<sub>2</sub> flux trends (Methods, Extended Data Fig. 2), indicating that a clean separation of forced trends from trends driven by internal variability is not possible with the CMIP5 multi-model ensemble, as it is with CESM-LE.

Our model analysis considers forced trends and the spread of internal trends in the ocean carbon sink across timeframes from decadal to centennial, all starting in 1990. Forced trends are shown only if they can be distinguished from trends due to internal variability with 95% confidence<sup>14</sup> (Methods).

For the decade starting in 1990, internal variability is large enough to preclude identification of forced trends in the carbon sink across most

of the ocean (Fig. 2a). Internally driven variability in trends (Fig. 2d) is largest in the equatorial Pacific due to El Niño/Southern Oscillation effects, and in regions of strong seasonal and interannual climate variability, such as the high latitudes of the North Pacific and Atlantic and north of seasonal sea ice in the Southern Ocean<sup>5,8,10,11,13,22,27,28</sup>. Only in the subpolar North Atlantic, equatorial Atlantic and in some locations in the Southern Ocean are forced trends large enough to emerge from the variability over this period, and in these locations CO<sub>2</sub> uptake increases (Fig. 2a).

As a result of anthropogenic CO<sub>2</sub> emissions from 1990–2019, the ocean carbon sink increases in most locations outside the subtropics

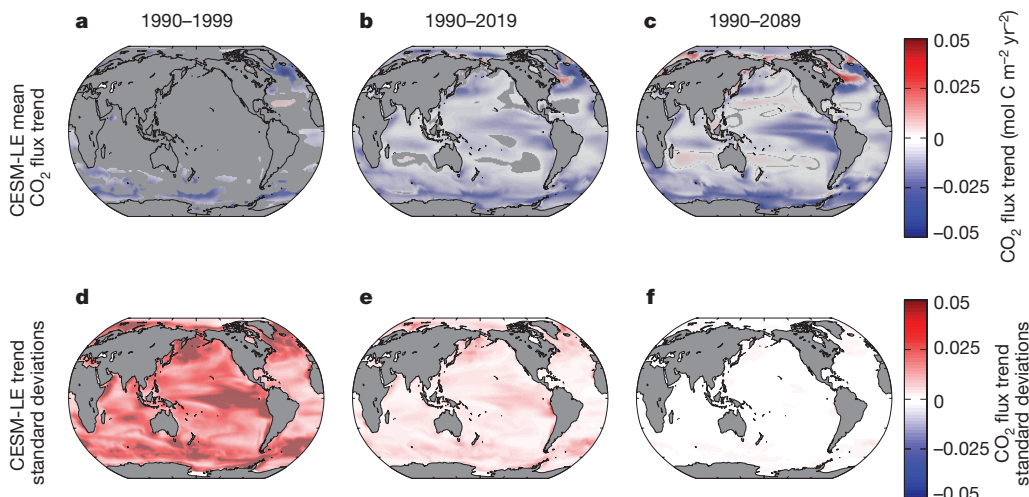


**Figure 2 | Forcet trends and internal variability of CESM-LE trends in sea-to-air CO<sub>2</sub> flux.** Forcet trends for **a**, 1990–1999, **b**, 1990–2019 and **c**, 1990–2089. Light-grey ocean areas show where the forced trend cannot be identified with 95% confidence (Methods). CO<sub>2</sub> flux trend standard

deviations, indicating the impact of internal variability on CO<sub>2</sub> flux trends, for **d**, 1990–1999, **e**, 1990–2019 and **f**, 1990–2089. Negative values indicate increasing ocean carbon uptake.

(Fig. 2b). In isolated regions within the subtropics, the forced trend in carbon uptake for 1990–2019 is not large enough to be identifiable at the 95% level, despite the fact that internally driven variability is substantially reduced relative to the decadal timeframe (Fig. 2d, e). Over 100 years (1990–2089), anthropogenic forcing leads to strong increases in uptake in the high latitudes, and to reduced outgassing in the equatorial Pacific and the eastern upwelling zones off South America and Africa. In the Pacific and Indian subtropics, the forced trend illustrates weakened carbon uptake by 2100 (Fig. 2c). Internal variability has minimal impact on 100-year CO<sub>2</sub> flux trends (Fig. 2f).

The ocean's capacity to absorb increasing amounts of anthropogenic CO<sub>2</sub> is not uniformly distributed. Across multi-decadal to centennial timescales, CO<sub>2</sub> flux does not change or decreases in the subtropical gyres (Fig. 2b, c). This is consistent with a convergent large-scale circulation and strong stratification that isolates the surface from the deep ocean's large capacity to hold carbon. Long-term warming also reduces CO<sub>2</sub> solubility<sup>10,13,16</sup>. In contrast, the regions where ocean carbon uptake strongly increases are those with strong exchange between the surface and the deep ocean. In the equatorial Pacific, in eastern boundary zones, and in the Southern Ocean, upwelling deep waters have been out of contact with the atmosphere for hundreds of years and thus hold little, if any, anthropogenic carbon. As time progresses, upwelling waters encounter an ever-higher atmospheric p<sub>CO<sub>2</sub></sub>, which diminishes outgassing of natural carbon<sup>4,22,28</sup> (Extended Data Fig. 1). In the North Atlantic, the direction of the exchange with the deep is reversed, with surface waters being transformed into deep waters by rapid buoyancy loss and deep convection. During this transformation, these waters increasingly absorb more carbon as atmospheric p<sub>CO<sub>2</sub></sub> rises. There is a large-scale correspondence of the regions of mean carbon uptake at present<sup>3</sup> with the regions where carbon uptake is predicted to grow most rapidly in the twenty-first century.

The ability to separate forced from internal trends in CESM-LE (Fig. 2) allows for an assessment of timescales over which observations would be required in order to detect anthropogenically driven change in ocean carbon uptake from observations (Fig. 3). Consistent with previous studies<sup>26,29</sup>, detectability is assessed using 'time of emergence' which is the year in which the signal of the forced trend would emerge from the noise of the internal variability. This analysis assumes observations began in 1990 (Methods).

The forced trend emerges early (by 2010) in some of the Southern Ocean and the Atlantic, where there is a large short-term change in the sink. Given the strong internal variability and the smaller forced trend in the equatorial Pacific, time of emergence is generally intermediate here (by 2030–2050). The latest emergence occurs in the Pacific and Indian subtropical regions (2050+). Where the net effect of the forcing is to drive long-term steady carbon uptake, no change should be detected before 2100 (white areas in Fig. 3). If internal variability were to be substantially underestimated or overestimated at a location, estimates of time of emergence would be too short or too long, respectively. However, comparison with data indicates that CESM-LE captures carbon cycle variability reasonably well (Extended Data Tables 1 and 2).

Using our current observational system for surface ocean carbon, should we be able to detect these predicted changes? At seven ocean time series stations, direct measurements of the ocean carbon cycle have been made at quarterly to monthly intervals for one to several decades<sup>9</sup> (Fig. 3). In the Atlantic, these locations are situated such that if observations had occurred since 1990 at a frequency sufficient to constrain the annual mean flux, they should be able to reveal change in the ocean carbon sink as distinct from internal variability at present (Irminger Sea, by 2015) or in the near future (BATS, ESTOC, CARIACO, by 2020; Iceland Sea, by 2040) (Fig. 3). However, for the Pacific sites, detection of change in carbon uptake should not be expected until at least 2050 (HOT, by 2050; Munida, beyond 2100). Unfortunately, at the time series site where CESM-LE suggests the forced trend may be first detectable (Irminger Sea), the p<sub>CO<sub>2</sub></sub> data set is short (1983–2005) and highly variable<sup>9</sup>, making it

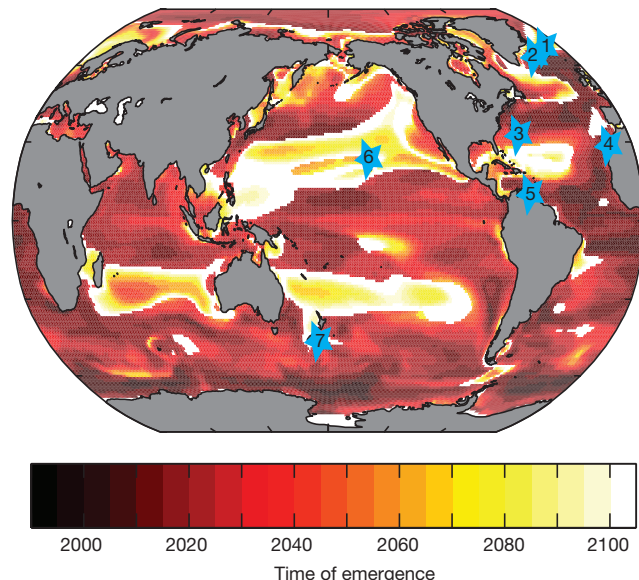


**Figure 3 | Time of emergence for sea-to-air CO<sub>2</sub> flux.** Time of emergence is when the forced trend becomes detectable given the internal variability (Methods). Blue stars indicate seven ocean timeseries stations<sup>9</sup>, from North to South in the Atlantic: (1) Iceland Sea, (2) Irminger Sea, (3) Bermuda Atlantic Time-series Study (BATS), (4) European Station for Time series in the Ocean at the Canary Islands (ESTOC), (5) Carbon Retention In A Colored Ocean (CARIACO) and from North to South in the Pacific, (6) Hawaii Ocean Time-series (HOT) and (7) Munida. Mean times of emergence for each biome are presented in Extended Data Table 4.

impossible to determine if a trend towards increasing carbon flux is, in fact, occurring.

Surface ocean carbon data from volunteer commercial and scientific ships are presently too sparse for direct estimation of multi-decadal carbon cycle trends in most regions<sup>5,8,10,12</sup>. However, in the subtropics of the North Atlantic and Pacific, there are sufficient data to indicate a steady ocean carbon sink, and in the equatorial Atlantic to indicate an increasing sink for 1981–2009<sup>10</sup>. These changes are consistent with the 30-year forced signals expected from CESM-LE (Fig. 2b). More data, from all sources, will be required to determine whether these signals are, in fact, illustrating the forced trend in ocean carbon uptake<sup>10</sup>.

Going forward, ocean carbon monitoring efforts can benefit from this new ability to separate internal variability from forced trends. Long-term records can be interpreted in the context of the expected forced change in the ocean carbon sink; monitoring can be targeted to regions where the largest forced changes are expected; and regional aggregation approaches that optimally seek the forced signal can be developed. Concurrently, expansion of these analyses to large ensembles of other Earth system models<sup>18,26</sup> will further elucidate the mechanisms, magnitudes, and timescales of forced trends in the ocean carbon sink.

**Online Content** Methods, along with any additional Extended Data display items and Source Data, are available in the online version of the paper; references unique to these sections appear only in the online paper.

**Received 10 April; accepted 21 December 2015.**

1. Khatiwala, S., Primeau, F. & Hall, T. Reconstruction of the history of anthropogenic CO<sub>2</sub> concentrations in the ocean. *Nature* **462**, 346–349 (2009).
2. Ciais, P. & Sabine, C. in *Climate Change. The Physical Science Basis. Contribution of Working Group I to the Fifth Assessment Report of the Intergovernmental Panel on Climate Change* (eds Stocker, T. F. et al.) Ch. 6, 1535 (Cambridge Univ. Press, 2013).
3. Gruber, N. et al. Oceanic sources, sinks, and transport of atmospheric CO<sub>2</sub>. *Glob. Biogeochem. Cycles* **23**, GB1005 (2009).
4. Takahashi, T. et al. Climatological mean and decadal change in surface ocean pCO<sub>2</sub>, and net sea-air CO<sub>2</sub> flux over the global oceans. *Deep Sea Res. Part II* **56**, 554–577 (2009).

5. Landschützer, P. *et al.* The reinvigoration of the Southern Ocean carbon sink. *Science* **349**, 1221–1224 (2015).
6. Schuster, U. *et al.* An assessment of the Atlantic and Arctic sea-air CO<sub>2</sub> fluxes, 1990–2009. *Biogeosciences* **10**, 607–627 (2013).
7. Randerson, J. T. *et al.* Multicentury changes in ocean and land contributions to the climate-carbon feedback. *Glob. Biogeochem. Cycles* **29**, 744–759 (2015).
8. Munro, D. R. *et al.* Recent evidence for a strengthening CO<sub>2</sub> sink in the Southern Ocean from carbonate system measurements in the Drake Passage (2002–2015). *Geophys. Res. Lett.* **42**, 7623–7630 (2015).
9. Bates, N. *et al.* A time-series view of changing ocean chemistry due to ocean uptake of anthropogenic CO<sub>2</sub> and ocean acidification. *Oceanography* **27**, 126–141 (2014).
10. Fay, A. R. & McKinley, G. A. Global trends in surface ocean pCO<sub>2</sub> from in situ data. *Glob. Biogeochem. Cycles* **27**, 541–557 (2013).
11. McKinley, G. A., Fay, A. R., Takahashi, T. & Metzl, N. Convergence of atmospheric and North Atlantic carbon dioxide trends on multidecadal timescales. *Nature Geosci.* **4**, 606–610 (2011).
12. Le Quéré, C., Raupach, M. R., Canadell, J. G. & Al, G. M. E. Trends in the sources and sinks of carbon dioxide. *Nature Geosci.* **2**, 831–836 (2009).
13. Le Quéré, C., Takahashi, T., Buitenhuis, E. T., Rödenbeck, C. & Sutherland, S. C. Impact of climate change and variability on the global oceanic sink of CO<sub>2</sub>. *Glob. Biogeochem. Cycles* **24**, GB4007 (2010).
14. Deser, C., Phillips, A., Bourdette, V. & Teng, H. Uncertainty in climate change projections: the role of internal variability. *Clim. Dyn.* **38**, 527–546 (2012).
15. DeVries, T. The oceanic anthropogenic CO<sub>2</sub> sink: storage, air-sea fluxes, and transports over the industrial era. *Glob. Biogeochem. Cycles* **28**, 631–647 (2014).
16. Sarmiento, J. L. & LeQuéré, C. Oceanic carbon dioxide uptake in a model of century-scale global warming. *Science* **274**, 1346–1350 (1996).
17. Deser, C., Knutti, R., Solomon, S. & Phillips, A. S. Communication of the role of natural variability in future North American climate. *Nature Clim. Change* **2**, 775–779 (2012).
18. Frölicher, T. L., Joos, F., Plattner, G.-K., Steinacher, M. & Doney, S. C. Natural variability and anthropogenic trends in oceanic oxygen in a coupled carbon cycle-climate model ensemble. *Glob. Biogeochem. Cycles* **23**, GB1003 (2009).
19. Ullman, D. J., McKinley, G. A., Bennington, V. & Dutkiewicz, S. Trends in the North Atlantic carbon sink: 1992–2006. *Glob. Biogeochem. Cycles* **23**, GB4011 (2009).
20. Lovenduski, N. & Gruber, N. Toward a mechanistic understanding of the decadal trends in the Southern Ocean carbon sink. *Glob. Biogeochem. Cycles* **22**, GB3016 (2008).
21. Long, M. C., Lindsay, K., Peacock, S., Moore, J. K. & Doney, S. C. Twentieth-century oceanic carbon uptake and storage in CESM1 (BGC). *J. Clim.* **26**, 6775–6800 (2013).
22. Resplandy, L., Séférian, R. & Bopp, L. Natural variability of CO<sub>2</sub> and O<sub>2</sub> fluxes: what can we learn from centuries-long climate models simulations? *J. Geophys. Res.* **120**, 384–404 (2015).
23. Frölicher, T. L. *et al.* Dominance of the Southern Ocean in anthropogenic carbon and heat uptake in CMIP5 models. *J. Clim.* **28**, 862–886 (2015).
24. Hawkins, E. & Sutton, R. The potential to narrow uncertainty in regional climate predictions. *Bull. Am. Meteorol. Soc.* **90**, 1095–1107 (2009).
25. Kay, J. E. *et al.* The Community Earth System Model (CESM) Large Ensemble Project: a community resource for studying climate change in the presence of internal climate variability. *Bull. Am. Meteorol. Soc.* **96**, 1333–1349 (2014).
26. Rodgers, K. B., Lin, J. & Frölicher, T. L. Emergence of multiple ocean ecosystem drivers in a large ensemble suite with an Earth system model. *Biogeosciences* **12**, 3301–3320 (2015).
27. Lovenduski, N. S., Fay, A. R. & McKinley, G. A. Observing multi-decadal trends in Southern Ocean CO<sub>2</sub> uptake: what can we learn from an ocean model? *Glob. Biogeochem. Cycles* **29**, 416–426 (2015).
28. Landschützer, P., Gruber, N., Bakker, D. C. E. & Schuster, U. Recent variability of the global ocean carbon sink. *Glob. Biogeochem. Cycles* **28**, 927–949 (2014).
29. Hawkins, E. & Sutton, R. Time of emergence of climate signals. *Geophys. Res. Lett.* **39**, L01702 (2012).

**Acknowledgements** The National Science Foundation sponsors National Center for Atmospheric Research, where the Community Earth System Model is developed. Computing resources were provided by the Climate Simulation Laboratory at NCAR's Computational and Information Systems Laboratory, sponsored by the NSF and other agencies. NCAR's Advanced Study Program sponsored D.J.P., K.L., M.C.L. and G.A.M. to initiate this analysis. We also thank NASA for funding (grants NNX11AF53G and NNX13AC53G to G.A.M., D.J.P., A.R.F. and N.S.L.). N.S.L. also thanks the NSF (grant OCE-1155240) and NOAA (grant NA12OAR4310058).

**Author Contributions** G.A.M. conceived the analysis, which was further refined by all authors. K.L. coordinated inclusion of ocean biogeochemistry in CESM-LE. D.J.P. and A.R.F. did the analysis. All authors discussed results and contributed to writing the manuscript.

**Author Information** Reprints and permissions information is available at [www.nature.com/reprints](http://www.nature.com/reprints). The authors declare no competing financial interests. Readers are welcome to comment on the online version of the paper. Correspondence and requests for materials should be addressed to G.A.M. ([gamckinley@wisc.edu](mailto:gamckinley@wisc.edu)).

## METHODS

**The Large Ensemble of the Community Earth System Model.** The Community Earth System Model (CESM) is a comprehensive coupled climate model consisting of atmosphere, ocean, land surface, and sea ice component models<sup>30</sup>. The ocean physical model is the ocean component of the Community Climate System Model version 4<sup>31</sup>. The model has nominal 1° horizontal resolution and 60 vertical levels. Mesoscale eddy transport, diapycnal mixing, and mixed layer restratification by submesoscale eddies are parameterized with state-of-the-art approaches. The biogeochemical–ecosystem ocean model includes multi-nutrient co-limitation on phytoplankton growth and specific phytoplankton functional groups as well as full-depth ocean carbonate system thermodynamics, sea-to-air CO<sub>2</sub> fluxes, and a dynamic iron cycle<sup>30</sup>. The biogeochemical–ecosystem model compares favourably to observations, though there are some important biases, including weak Southern Ocean CO<sub>2</sub> uptake<sup>21</sup>.

The CESM-LE began with a multi-century 1850 control simulation with constant pre-industrial forcing; the ocean physical state was initialized from observations, ocean biogeochemical tracers were initialized from a separate 600-year spin-up, and other component models were initialized from previous CESM1 simulations. Once the control simulation climate achieved quasi-equilibrium with the 1850 forcing, the first ensemble member was initialized from a randomly selected year in the 1850 control run: 1 January, model year 402. Ensemble member 1 was integrated forward from 1850 to 2100. The remaining ensemble members were integrated from 1920 to 2100 using slightly different initial conditions: Ensemble member 2 used one-day lagged ocean initial conditions, while spread in the remaining ensemble members was generated by round-off level perturbations to their initial air temperature fields<sup>25</sup>. After initial condition memory was lost, each ensemble member evolved independently. A total of 38 ensemble members were generated in this fashion, but 6 of these had corrupted ocean biogeochemical output due to a setup error and affected fields were discarded. All ensemble members have the same specified external forcing: historical forcing from 1920 to 2005, and RCP8.5 forcing from 2006 to 2100. Differences from observed atmospheric  $p_{\text{CO}_2}$  for RCP8.5 for the 2006–2014 period are minimal<sup>32</sup>. Since atmospheric CO<sub>2</sub> concentrations are prescribed, CESM-LE ocean carbon fluxes do not feed back on the modelled climate.

**Analysis methods.** We consider the linear trend at each model gridcell of annual mean CO<sub>2</sub> flux, in units of moles of carbon per square metre per year squared. The trend for CO<sub>2</sub> flux is calculated for each ensemble member. The forced trend is the average trend across the 32 ensembles. Each ensemble member's unforced (internal) trend, due to internal variability, is the difference between that ensemble's trend and the forced trend. The 95% confidence level for identification of the forced trend is calculated, for each grid cell and time frame, based on the number of ensembles required to resolve the ensemble mean response:  $N_{\min} = 8/(X/\sigma)^2$ , where X is the forced trend and  $\sigma$  is the standard deviation of trends<sup>14</sup>. If  $N_{\min}$  exceeds the number of ensembles in CESM-LE ( $N_{\text{ensembles}} = 32$ ), the forced trend cannot be identified with 95% confidence. Time of emergence is the first year in which the signal-to-noise ratio exceeds a threshold value of 2, where the signal is the forced trend and the noise is the ensemble standard deviation<sup>29</sup>. For efficiency of computation and presentation, signal-to-noise ratios are calculated at 5-year intervals (that is, 1990–1995, 1990–2000, 1990–2005, and so on). The signal-to-noise ratio must remain greater than 2 for all subsequent years.

**Model comparisons to observations.** To assess the representation of internal variability in CESM-LE, Extended Data Table 1 compares CESM-LE modelled to observed variability in annual mean  $p_{\text{CO}_2}$  and CO<sub>2</sub> flux for 1982–2011, and Extended Data Table 2 compares trends over the same period.  $p_{\text{CO}_2}$  data are from the Surface Ocean CO<sub>2</sub> Atlas (SOCATv2)<sup>33</sup> averaged to monthly means at 1° × 1° resolution. CESM-LE members are each sampled in  $p_{\text{CO}_2}$  to reflect the data density available in SOCATv2. A background mean climatology<sup>4</sup> is removed at 1° × 1° resolution in order to address the potential of spatial aliasing when averaging to biome-scale<sup>10,34,35</sup>. An area-weighted average is then used to arrive at biome-scale annual means, and the 30-year trend is removed before calculating the standard deviation. For the CO<sub>2</sub> flux, we utilize monthly 1° × 1° resolution flux estimates that have full spatial and temporal coverage over the period 1982–2011<sup>28</sup>. These estimates are based on the same  $p_{\text{CO}_2}$  data set (SOCATv2). With the full global coverage of the CO<sub>2</sub> flux product, there is no need to sample or to remove a background climatology from CESM-LE before biome averaging. Otherwise, the same processing is employed as for  $p_{\text{CO}_2}$ . The uncertainty reported in Extended Data Table 1 is one standard deviation of the variability represented by the 32 CESM-LE members for each variable. There is insufficient data to make an independent uncertainty estimate with respect to variability from the observations. In Extended Data Table 2, linear trends in observed annual mean  $p_{\text{CO}_2}$  and CESM-LE  $p_{\text{CO}_2}$ , sampled in the same way as these observations, are compared. Sampling in the same way as the observations allows for a direct model-to-observation

comparison in spite of the fact that the sparse data coverage may lead to inaccurate observed estimates of annual mean  $p_{\text{CO}_2}$  for some biomes in some years. Since the CO<sub>2</sub> flux product offers full coverage in space and time, there is no need for sampling prior to the calculation of trends.

Within the uncertainty, modelled  $p_{\text{CO}_2}$  variance is correct in seven of the biomes, underestimated in five biomes and overestimated in three biomes (Extended Data Table 1). However, in two of the three biomes where  $p_{\text{CO}_2}$  variability is overestimated by the model (SO STSS, SO SPSS), comparison to the CO<sub>2</sub> flux product suggests that the model underestimates variability. In the third (NP STPS), the flux product comparison indicates that the model appropriately simulates variability. Conversely, in the biomes where  $p_{\text{CO}_2}$  variability is underestimated, the CO<sub>2</sub> flux product comparison indicates either variability consistent with observations (NA STSS, EQ Atl), too high (NP STSS), or too low (NA SPSS, SA STPS). Similarly, in the biomes where  $p_{\text{CO}_2}$  variability is consistent with the observations, the CO<sub>2</sub> flux comparison indicates overestimation by the model (East EQ Pac, West EQ Pac, IND STPS), underestimation (NP SPSS, SO ICE), or consistency (SP STPS).

Modelled trends in  $p_{\text{CO}_2}$  and CO<sub>2</sub> flux (Extended Data Table 2) are largely consistent with observed trends, given the uncertainty. In one biome (West EQ Pac), the trend in  $p_{\text{CO}_2}$  in the model is overestimated, though in this biome the CO<sub>2</sub> flux trend is consistent with the observed estimates. In three biomes (NP STPS, East EQ Pac, IND STPS), the flux trend is too large, and in one (SO SPSS), it is too small. However, in all four of these biomes, the  $p_{\text{CO}_2}$  trends are consistent with the observed estimates. There is no clear relationship between over- and underestimation of trends and over- and underestimation of variability (Extended Data Table 1).

In the CESM-LE,  $p_{\text{CO}_2}$  variability and trends dominantly control CO<sub>2</sub> flux variability and trends<sup>21</sup>. Thus, the fact that these comparisons for  $p_{\text{CO}_2}$  and CO<sub>2</sub> flux variability and trends differ substantially suggests that there is additional, unquantified uncertainty driven by the sparse sampling for  $p_{\text{CO}_2}$  and assumptions made in the development of the flux product<sup>28</sup>. That CESM-LE falls clearly within the range of observed  $p_{\text{CO}_2}$  and estimated CO<sub>2</sub> flux variability and trends indicates that the model's representation of the carbon cycle is, on the whole, consistent with our current observational understanding. More observations are needed to better constrain internal variability and trends in the surface ocean carbon cycle.

**Forced trends in the CMIP5 ensemble.** Twelve CMIP5 Earth system models are included in the analysis in addition to the CESM-LE for the historical period. The CMIP5 models included are those models that report CO<sub>2</sub> flux at monthly timescales for a historical simulation through 2005 and with the RCP8.5 scenario for 2006–2100; see Extended Data Table 3 for included models. The CESM1-Biogeochemistry (CESM1-BGC) model included in the CMIP5 model suite is a predecessor to the CESM-LE.

Owing to the combined effect of a smaller number of ensemble members for CMIP5 and the larger variability across these ensembles (Extended Data Fig. 2d–f), due in part to structural differences<sup>29</sup>, the forced trend in CO<sub>2</sub> flux cannot be identified from CMIP5 across most of the global oceans, even for the time frame 1990–2089 (Extended Data Fig. 2a–c). Where the forced trend from CMIP5 is discernible, primarily in the equatorial Pacific and Southern Ocean, it is of the same sign as CESM-LE (increasing uptake) but of weaker magnitude.

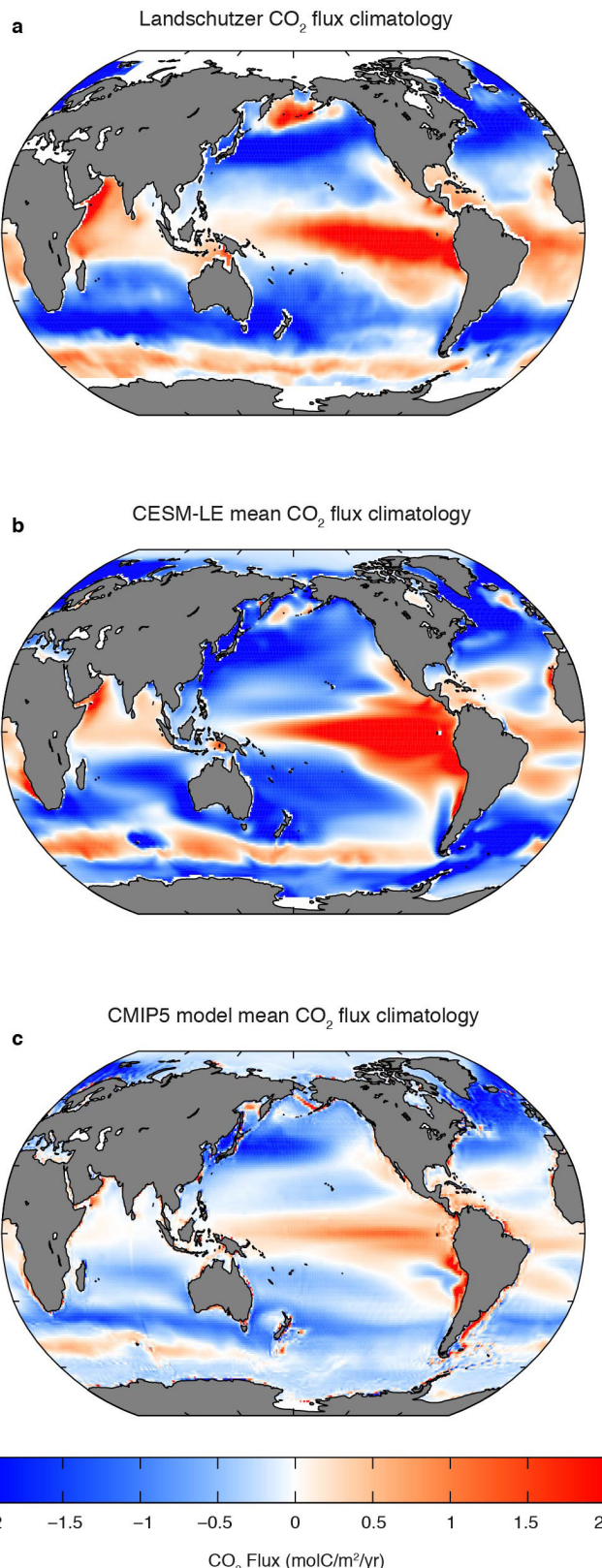
**Data sources.** Surface Ocean CO<sub>2</sub> Atlas (SOCAT v2)<sup>33</sup>  $p_{\text{CO}_2}$  data were taken from [www.socat.info/access.html](http://www.socat.info/access.html). CO<sub>2</sub> flux estimates<sup>28</sup> were obtained from [http://cdiac.esd.orl.gov/oceans/SPCO2\\_1982\\_2011\\_ETH\\_SOM\\_FFN.html](http://cdiac.esd.orl.gov/oceans/SPCO2_1982_2011_ETH_SOM_FFN.html).

**Model output sources.** CESM-LE<sup>25</sup> is available from [https://www.earthsystemgrid.org/dataset/ucar.cgd.ccsm4.CESM\\_CAM5\\_BGC\\_LE.html](https://www.earthsystemgrid.org/dataset/ucar.cgd.ccsm4.CESM_CAM5_BGC_LE.html). CMIP5<sup>36</sup> is available from [http://www.ipcc-data.org/sim/gcm\\_monthly/AR5/WG1-Archive.html](http://www.ipcc-data.org/sim/gcm_monthly/AR5/WG1-Archive.html).

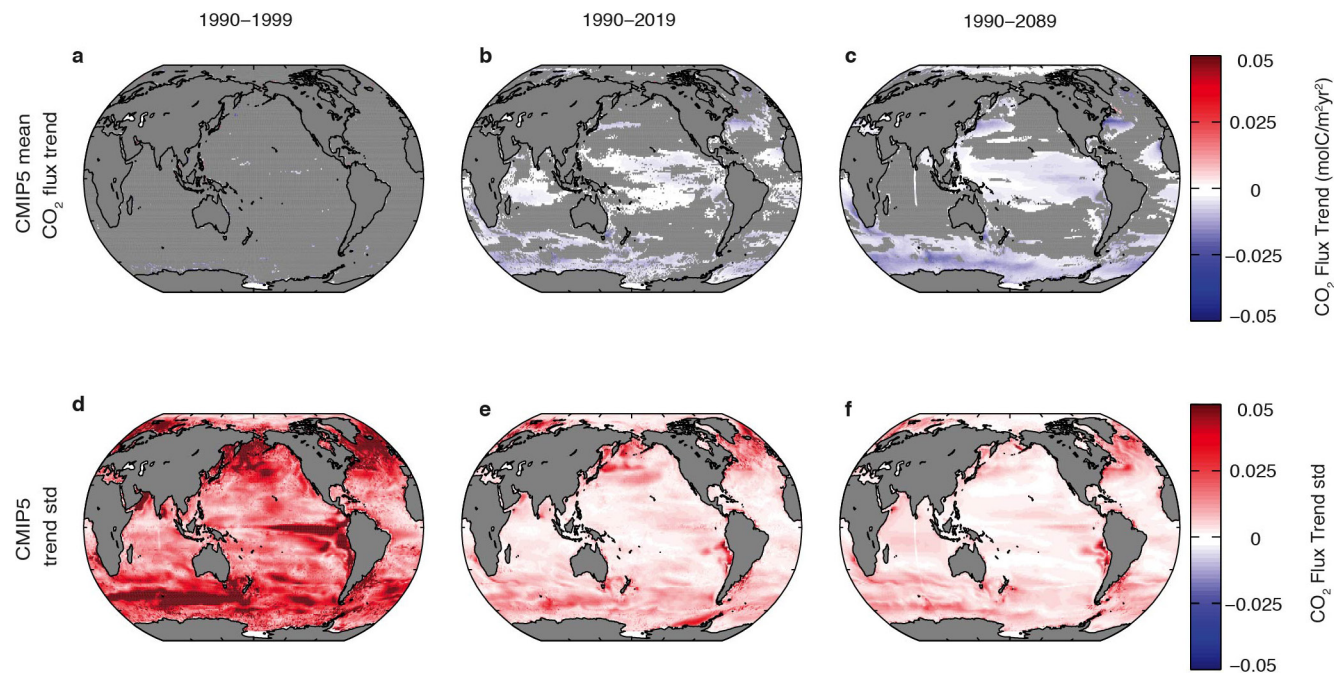
**Code availability.** Code for analysis and production of figures is available upon request. Please contact G.A.M. (gamckinley@wisc.edu).

30. Hurrell, J. W. et al. The community earth system model: a framework for collaborative research. *Bull. Am. Meteorol. Soc.* **94**, 1339–1360 (2013).
31. Moore, J. K. et al. Marine ecosystem dynamics and biogeochemical cycling in the Community Earth System Model [CESM1 (BGC)]: comparison of the 1990s with the 2090s under the RCP4.5 and RCP8.5 scenarios. *J. Clim.* **26**, 9291–9312 (2013).
32. Danabasoglu, G. S. C. et al. The CCSM4 Ocean Component. *J. Clim.* **25**, 1361–1389 (2012).
33. Bakker, D. C. E. et al. An update to the surface ocean CO<sub>2</sub> atlas (SOCAT version 2). *Earth Syst. Sci. Data* **6**, 69–90 (2014).
34. Fay, A. R. & McKinley, G. A. Global open-ocean biomes: mean and temporal variability. *Earth Syst. Sci. Data* **6**, 273–284 (2014).
35. Fay, A. R., McKinley, G. A. & Lovenduski, N. S. Southern Ocean carbon trends: sensitivity to methods. *Geophys. Res. Lett.* **41**, 6833–6840 (2014).
36. Taylor, K. E., Stouffer, R. J. & Meehl, G. A. An overview of CMIP5 and the experiment design. *Bull. Am. Meteorol. Soc.* **93**, 485–498 (2012).

37. Chylek, P., Li, J., Dubey, M. K., Wang, M. & Lesins, G. Observed and model simulated 20th century Arctic temperature variability: Canadian Earth System Model CanESM2. *Atmos. Chem. Phys. Discuss.* **11**, 22893–22907 (2011).
38. Collins, W. J. *et al.* Development and evaluation of an Earth-system model—HadGEM2. *Geosci. Model Dev.* **4**, 1051–1075 (2011).
39. Dufresne, J.-L. *et al.* Climate change projections using the IPSL-CM5 Earth System Model: from CMIP3 to CMIP5. *Clim. Dyn.* **40**, 2123–2165 (2013).
40. Dunne, J. P. *et al.* GFDL's ESM2 global coupled climate-carbon Earth System Models. Part I: physical formulation and baseline simulation characteristics. *J. Clim.* **25**, 6646–6665 (2012).
41. Fogli, P. G. *et al.* INGV-CMCC carbon (ICC): a carbon cycle earth system model. *CMCC Res. Pap.* 61, <http://ssrn.com/abstract=1517282> (Social Science Research Network, 2009).
42. Giorgetta, M. *et al.* CMIP5 simulations of the Max Planck Institute for Meteorology (MPI-M) based on the MPI-ESM-LR model: the historical experiment. <http://dx.doi.org/10.1594/WDCC/CMIP5.MXELhi> (World Data Centre for Climate, Earth System Grid Federation, 2012).
43. Giorgetta, M. *et al.* CMIP5 simulations of the Max Planck Institute for Meteorology (MPI-M) based on the MPI-ESM-LR model: the RCP85 experiment. <http://dx.doi.org/10.1594/WDCC/CMIP5.MXELr8> (World Data Centre for Climate, Earth System Grid Federation, 2012).
44. Ji, D. *et al.* Description and basic evaluation of Beijing Normal University Earth System Model (BNU-ESM) version 1. *Geosci. Model Dev.* **7**, 2039–2064 (2014).
45. Lindsay, K. *et al.* Preindustrial-control and twentieth-century carbon cycle experiments with the Earth System Model CESM1 (BGC). *J. Clim.* **27**, 8981–9005 (2014).
46. Tjiputra, J. F. *et al.* Evaluation of the carbon cycle components in the Norwegian Earth System Model (NorESM). *Geosci. Model Dev.* **6**, 301–325 (2013).
47. Volodin, E. M., Dianskii, N. A. & Gusev, A. V. Simulating present-day climate with the INMCM4.0 coupled model of the atmospheric and oceanic general circulations. *Izv. Atmos. Ocean. Phys.* **46**, 414–431 (2010).
48. Watanabe, S. *et al.* MIROC-ESM 2010: model description and basic results of CMIP5-20c3m experiments. *Geosci. Model Dev.* **4**, 845–872 (2011).
49. Wu, T. *et al.* Global carbon budgets simulated by the Beijing Climate Center Climate System Model for the last century. *J. Geophys. Res.* **118**, 4326–4347 (2013).



**Extended Data Figure 1 | Comparison of 1982–2011 mean CO<sub>2</sub> flux.**  
a, Data-based climatology (ref. 28). b, CESM large ensemble 32-member mean. c, Mean of 12 CMIP5 models.



**Extended Data Figure 2 | Forced trends and variability of CMIP5 trends in sea-to-air CO<sub>2</sub> flux.** Forced trends for **a**, 1990–1999, **b**, 1990–2019 and **c**, 1990–2089. Grey areas are where the forced trend cannot be distinguished from the variability with 95% confidence (Methods).

CO<sub>2</sub> flux trend standard deviations, indicating the impact of variability on CO<sub>2</sub> flux trends, for **d**, 1990–1999, **e**, 1990–2019 and **f**, 1990–2089. Negative values indicate increasing ocean carbon uptake.

Extended Data Table 1 | Comparison of observed and modelled  $p_{\text{CO}_2}$  and  $\text{CO}_2$  flux variability for 1982–2011

Biome	$p_{\text{CO}_2}$			$\text{CO}_2$ flux		
	Data variability ( $\mu\text{atm}$ )	CESM-LE mean variability ( $\mu\text{atm}$ )	Uncertainty ( $\mu\text{atm}$ )	Data-based variability ( $\text{molC/m}^2/\text{yr}$ )	CESM-LE mean variability ( $\text{molC/m}^2/\text{yr}$ )	Uncertainty ( $\text{molC/m}^2/\text{yr}$ )
NP SPSS	7.9	10.2	2.0	<u>0.42</u>	<u>0.13</u>	<u>0.02</u>
NP STSS	<u>7.3</u>	<u>5.9</u>	<u>0.4</u>	<u>0.09</u>	<u>0.13</u>	<u>0.01</u>
NP STPS	<u>4.2</u>	<u>5.4</u>	<u>0.5</u>	0.05	0.07	0.01
East EQ Pac	6.3	5.9	0.7	<u>0.07</u>	<u>0.15</u>	<u>0.02</u>
West EQ Pac	13.0	12.6	2.0	<u>0.23</u>	<u>0.36</u>	<u>0.05</u>
SP STPS	8.3	6.4	1.0	0.07	0.08	0.01
NA SPSS	<u>22.4</u>	<u>19.7</u>	<u>1.0</u>	<u>0.25</u>	<u>0.12</u>	<u>0.01</u>
NA STSS	<u>7.4</u>	<u>5.2</u>	<u>0.6</u>	0.10	0.10	0.02
NA STPS	<u>5.2</u>	<u>5.6</u>	<u>0.4</u>	<u>0.09</u>	<u>0.06</u>	<u>0.01</u>
EQ Atl	<u>8.8</u>	<u>6.5</u>	<u>0.6</u>	0.07	0.06	0.01
SA STPS	<u>9.7</u>	<u>8.5</u>	<u>0.5</u>	<u>0.10</u>	<u>0.06</u>	<u>0.007</u>
IND STPS	11.1	10.6	1.0	<u>0.04</u>	<u>0.10</u>	<u>0.01</u>
SO STSS	<u>5.9</u>	<u>12.4</u>	<u>2.0</u>	<u>0.14</u>	<u>0.08</u>	<u>0.01</u>
SO SPSS	<u>4.8</u>	<u>12.8</u>	<u>2.0</u>	<u>0.22</u>	<u>0.11</u>	<u>0.01</u>
SO ICE	15.4	17.0	2.0	<u>0.22</u>	<u>0.05</u>	<u>0.005</u>

Variability is the standard deviation of the annual means from 1982 to 2011. Uncertainty of the variability is the standard deviation of the variability estimates for each of the 32 CESM-LE ensemble members. Underlining indicates that the modelled variability is lower than the observed variability, and italics indicates that the modelled variability is higher than the observed variability, in both cases taking into account the model-estimated uncertainty.  $p_{\text{CO}_2}$  data are from ref. 33;  $\text{CO}_2$  flux data are from ref. 28.

Extended Data Table 2 | Comparison of observed and modelled  $p_{\text{CO}_2}$  and  $\text{CO}_2$  flux trends for 1982–2011

Biome	$p_{\text{CO}_2}$	$\text{CO}_2$ flux		
	Data trend ( $\mu\text{atm}/\text{yr}$ )	CESM-LE forced trend ( $\mu\text{atm}/\text{yr}$ )	Data-based trend ( $\text{molC}/\text{m}^2/\text{yr}^2$ )	CESM-LE forced trend ( $\text{molC}/\text{m}^2/\text{yr}^2$ )
NP SPSS	$1.18 \pm 0.42$	$1.59 \pm 0.41$	$-0.012 \pm 0.017$	$-0.004 \pm 0.002$
NP STSS	$1.99 \pm 0.32$	$2.16 \pm 0.24$	$-0.011 \pm 0.004$	$-0.008 \pm 0.002$
NP STPS	$1.76 \pm 0.19$	$2.01 \pm 0.24$	$-0.008 \pm 0.002$	$-0.004 \pm 0.001$
West EQ Pac	$1.21 \pm 0.28$	$1.67 \pm 0.15$	$-0.001 \pm 0.003$	$-0.005 \pm 0.002$
East EQ Pac	$1.43 \pm 0.60$	$1.74 \pm 0.37$	$-0.023 \pm 0.010$	$-0.005 \pm 0.004$
SP STPS	$1.17 \pm 0.41$	$1.54 \pm 0.26$	$-0.006 \pm 0.003$	$-0.003 \pm 0.001$
NA SPSS	$1.06 \pm 1.33$	$1.44 \pm 1.11$	$-0.014 \pm 0.11$	$-0.016 \pm 0.002$
NA STSS	$1.73 \pm 0.51$	$1.77 \pm 0.32$	$-0.014 \pm 0.004$	$-0.014 \pm 0.001$
NA STPS	$1.57 \pm 0.27$	$1.88 \pm 0.28$	$-0.006 \pm 0.004$	$-0.003 \pm 0.001$
EQ Atl	$1.48 \pm 0.45$	$1.50 \pm 0.30$	$-0.001 \pm 0.003$	$-0.005 \pm 0.001$
SA STPS	$0.92 \pm 0.53$	$1.49 \pm 0.44$	$-0.004 \pm 0.005$	$-0.005 \pm 0.001$
IND STPS	$2.35 \pm 0.73$	$2.55 \pm 0.65$	$-0.008 \pm 0.002$	$-0.003 \pm 0.001$
SO STSS	$2.00 \pm 0.29$	$1.57 \pm 0.59$	$-0.005 \pm 0.006$	$-0.007 \pm 0.001$
SO SPSS	$1.58 \pm 0.24$	$0.97 \pm 0.55$	$0.004 \pm 0.010$	$-0.010 \pm 0.001$
SO ICE	$1.42 \pm 0.84$	$0.51 \pm 0.85$	$-0.010 \pm 0.010$	$-0.016 \pm 0.001$

Underlining indicates that the modelled trend is lower than the observed trend, and italics indicate that the modelled trend is higher than the observed trend, given the uncertainty (95% trend confidence intervals). Trends are based on annual means.  $p_{\text{CO}_2}$  data are from ref. 33;  $\text{CO}_2$  flux data are from ref. 28.

Extended Data Table 3 | CMIP5 models used in this work

Modeling Group	Model Name	Citation
Beijing Climate Center (BCC), China Meteorological Administration, China	BCC-CSM1.1m	49
Beijing Normal University (BNU), China College of Global Change and Earth System Science, China	BNU-ESM	44
Canadian Centre for Climate Modeling and Analysis, Victoria BC, Canada	CanESM2	37
National Center for Atmospheric Research, USA	CESM1-BGC	45
Centro Euro-Mediterraneo sui Cambiamenti Climatici, Lecce, Italy	CMCC-ESM	41
NOAA Geophysical Fluid Dynamics Laboratory, USA	GFDL-ESM2M	40
Met Office Hadley Centre, UK	HadGEM2	38
Institut Pierre-Simon Laplace, IPSL Climate Modelling Centre, France	IPSL-CM5-MR	39
Institute for Numerical Mathematics, Russia	INM-CM4	47
Japan Agency for Marine-Earth Science and Technology, Atmosphere and Ocean Research Institute, The University of Tokyo, Japan	MIROC-ESM	48
Max-Planck-Institute for Meteorology, Germany	MPI-ESM-LR	42, 43
Norwegian Climate Centre, Norway	NorESM1-ME	46

See refs 37–49.

Extended Data Table 4 | Biome long names and mean time of emergence

Biome acronym	Biome long name	Mean Time of Emergence
NP SPSS	North Pacific subpolar seasonally stratified	2063
NP STSS	North Pacific subtropical seasonally stratified	2038
NP STPS	North Pacific subtropical permanently stratified biome	2069
West EQ Pac	West Pacific equatorial	2048
East EQ Pac	East Pacific equatorial	2031
SP STPS	South Pacific subtropical permanently stratified biome	2054
NA SPSS	North Atlantic subpolar seasonally stratified	2054
NA STSS	North Atlantic subtropical seasonally stratified	2030
NA STPS	North Atlantic subtropical permanently stratified biome	2051
EQ Atl	Atlantic equatorial	2018
SA STPS	South Atlantic subtropical permanently stratified biome	2027
IND STPS	Indian subtropical permanently stratified biome	2048
SO STSS	Southern Ocean subtropical seasonally stratified	2032
SO SPSS	Southern Ocean subpolar seasonally stratified	2029
SO ICE	Southern Ocean marginal sea ice	2018

Names are taken from ref. 34.